

Fatigue Hysteresis of Carbon Fiber-Reinforced Ceramic-Matrix Composites at Room and Elevated Temperatures

Longbiao Li¹

Received: 11 May 2015 / Accepted: 13 May 2015 / Published online: 28 May 2015
© Springer Science+Business Media Dordrecht 2015

Abstract When the fiber-reinforced ceramic-matrix composites (CMCs) are first loading to fatigue peak stress, matrix multicroacking and fiber/matrix interface debonding occur. Under fatigue loading, the stress–strain hysteresis loops appear as fiber slipping relative to matrix in the interface debonded region upon unloading/reloading. Due to interface wear at room temperature or interface oxidation at elevated temperature, the interface shear stress degrades with increase of the number of applied cycles, leading to the evolution of the shape, location and area of stress–strain hysteresis loops. The evolution characteristics of fatigue hysteresis loss energy in different types of fiber-reinforced CMCs, i.e., unidirectional, cross-ply, 2D and 2.5D woven, have been investigated. The relationships between the fatigue hysteresis loss energy, stress–strain hysteresis loops, interface frictional slip, interface shear stress and interface radial thermal residual stress, matrix stochastic cracking and fatigue peak stress of fiber-reinforced CMCs have been established.

Keywords Ceramic-matrix composites (CMCs) · Fatigue · Hysteresis loops

1 Introduction

Ceramic materials possess high strength and modulus at elevated temperature. But their use as structural components is severely limited because of their brittleness. The continuous fiber-reinforced ceramic-matrix composites (CMCs), by incorporating fibers in ceramic matrices, however, not only exploit their attractive high-temperature strength but also reduce the propensity for catastrophic failure. These materials have already been implemented on some aero engines' components [1]. The CMC flaps for exhaust nozzles of SNECMA M53 and

✉ Longbiao Li
llb451@nuaa.edu.cn

¹ College of Civil Aviation, Nanjing University of Aeronautics and Astronautics, No. 29, Yudao St., Nanjing 210016, People's Republic of China

M88 aero engines have been used for more than one decade [2]. The CMC turbine vanes have been designed and tested in the aero engine environment under the implementation of Ultra Efficient Engine Technology (UEET) program [3]. A CMC turbine blade has been tested for 4 h by General Electric in a modified GE F414 engine, which represents the first application of CMC material in a rotating engine component. By incorporating the CMC turbine blades on a GE90-sized engine, the overall weight can be reduced by 455 kg, which represents ~6 % of dry weight of a full sized GE90–115 [4]. The CMC combustion chamber floating wall tiles have also been tested in the aero engine environment for 30 min, with the temperature range of 1047~1227 °C and the pressure of 2 MPa [5].

Under fatigue loading of fiber-reinforced CMCs, matrix multicracking and fiber/matrix interface debonding occur first [6], and the open and closure of matrix cracking upon each cycle is the basic fatigue damage mechanism [7]. The stress–strain hysteresis loops appear as fiber slipping relative to matrix in the interface debonded region upon unloading/reloading [8]. Marshall and Evans [9] first observed the hysteresis loops in unidirectional CMCs at room temperature and attributed to frictional slip between fibers and matrix. Holmes and Cho [10] investigated the fatigue hysteresis loops evolution characteristics of unidirectional SiC/CAS–II composite at room temperature. At the initial stage, the hysteresis modulus decreases rapidly, and the hysteresis loops area increases, due to matrix multicracking, fiber/matrix interface debonding and interface wear. When the cycle number approaches a critical value, the hysteresis modulus remains constant. However, the hysteresis loops area continually decreases with increase of the cycle number. Upon approaching fatigue fracture, the hysteresis loops area increases rapidly. Li [11] investigated the fatigue hysteresis behavior of cross-ply C/SiC composite at room temperature and 800 °C in air atmosphere. The hysteresis loops area decreases with increase of the cycle number. Reynaud [12] investigated the fatigue hysteresis loops evolution of two different types of CMCs at 600, 800 and 1000 °C in inert atmosphere. First, the hysteresis loops area of 2D SiC/SiC composite increases with increase of the number of applied cycles due to interface radial thermal residual compressive stress. The second ceramic composite, [0/90]_s SiC/MAS–L, the hysteresis loops area decreases with increase of the number of applied cycles due to interface radial thermal residual tensile stress. Fantozzi et al. [13] investigated the fatigue hysteresis loops evolution of 2.5D SiC/[Si–B–C] and 2.5D C/[Si–B–C] composites at 1200 °C in air atmosphere. The hysteresis loops area of 2.5D SiC/[Si–B–C] composite decreases with increase of the number of applied cycles due to interface wear; the hysteresis loops area of 2.5D C/[Si–B–C] composite decreases significantly after 144 h static fatigue loading attributed to PyC interface recession by oxidation or by a beginning of carbon fibers recession.

Many researchers investigated the fatigue hysteresis loops models of fiber-reinforced CMCs. Kotil et al. [14] first performed an investigation on the effect of interface shear stress on the shape and area of loading/unloading tensile hysteresis loops in unidirectional CMCs. Cho et al. [15] classified the interface frictional slip into two cases, i.e., the interface partially slip and interface completely slip, and obtained the hysteresis energy dissipation rate for two interface slip cases in unidirectional CMCs. Pryce and Smith [16] investigated the loading/unloading tensile hysteresis loops in unidirectional SiC/CAS composite when interface partially debonded based on the assumption of purely frictional load transfer between fibers and matrix. Ahn and Curtin [17] investigated the effect of matrix stochastic cracking on loading/unloading tensile hysteresis loops of unidirectional CMCs by assuming two-parameter Weibull distribution of matrix flaws and compared with Pryce–Smith model [16]. Solti et al. [18, 19] investigated the cyclic loading/unloading hysteresis loops in unidirectional and cross-ply

CMCs when interface was chemically bonded and partially debonded by adopting the maximum interface shear strength criterion to determine interface slip lengths, i.e., the interface debonded length, interface counter-slip length and interface new-slip length. Vagaggini et al. [20] developed the cyclic loading/unloading hysteresis loops models of unidirectional CMCs based on Hutchinson–Jenson fiber pull-out model [21], and investigated the effect of interface debonded energy on the stress–strain hysteresis loops. Li et al. investigated the effects of interface debonding [22], fiber Poisson contraction [23], fibers fracture [24] and matrix multicroacking [25, 26] on cyclic loading/unloading hysteresis loops of unidirectional and cross-ply CMCs. Fantozzi et al. [13] investigated the fatigue hysteresis behavior of bi- or multi-directional (cross-weave, cross-ply, 2.5D, [0/+60/−60]_n) with SiC or C long fibers reinforced SiC, MAS–L, Si–B–C or C matrix at room and elevated temperatures in inert or oxidation conditions.

Under cyclic fatigue loading, the stress applied oscillates between a valley stress and a peak stress. During each loading/unloading cycle, the fatigue behavior of fiber-reinforced CMCs can be described by a stress–strain loop where the area is the energy dissipated during each corresponding cycle. The evolution characteristics of fatigue hysteresis loss energy in different types of CMCs, i.e., unidirectional C/SiC, SiC/CAS, SiC/CAS–II and SiC/1723, cross-ply C/SiC, SiC/CAS, and SiC/MAS–L, 2D SiC/SiC, 2.5D C/SiC CMCs at room and elevated temperatures, have been investigated. The relationships between the hysteresis loss energy, stress–strain hysteresis loops, interface frictional slip, interface shear stress and interface radial thermal residual stress, matrix stochastic cracking and fatigue peak stress of CMCs with different fiber preforms have been established.

2 Hysteresis Loops Models of CMCs

If matrix cracking and fiber/matrix interface debonding are present upon first loading, the stress–strain hysteresis loops would develop as a result of energy dissipation through frictional slip between fibers and matrix upon unloading/reloading. The shape, area and location of cyclic loading/unloading stress–strain hysteresis loops depend upon fiber preforms, interface debonding, interface slip, interface thermal residual stress, matrix crack spacing and fatigue peak stress.

For a unidirectional composite, the fatigue peak stress σ_t at which the interface completely slips and the interface partially debonds upon unloading/reloading, is

$$\sigma_t = \frac{2V_f E_c \tau_i}{\rho V_m E_m} \left[1 + \sqrt{1 + \frac{4V_m E_m E_f \rho^2}{r_f E_c} \frac{\zeta_d}{\tau_i^2}} \right] - \sigma_{\min} \quad (1)$$

where V_f and V_m denote the fiber and matrix volume fraction, respectively; E_f , E_m and E_c denote the fiber, matrix and composite elastic modulus, respectively; τ_i and ζ_d denote the fiber/matrix interface shear stress and interface debonded energy; ρ denotes the shear-lag parameter; r_f denotes the fiber radius; and σ_{\min} denotes the valley stress.

The fatigue peak stress σ_p at which the interface completely slips and the interface completely debonds upon unloading/reloading, is

$$\sigma_p = 2 \frac{V_f E_c}{V_m E_m} \frac{L}{r_f} \tau_i + \sigma_{\min} \quad (2)$$

where L denotes the matrix crack spacing.

The interface completely debonded stress σ_b is

$$\sigma_b = \frac{V_f E_c \tau_i}{\rho V_m E_m} \left[1 + \rho \frac{L}{r_f} + \sqrt{1 + 4 \frac{V_m E_m E_f \rho^2}{r_f E_c \tau_i^2} \zeta_d} \right] \tag{3}$$

When $\sigma_{max} < \sigma_b$, the interface counter-slip length y and interface new-slip length z are affected by interface debonding, i.e., upon unloading to σ_{tr_pu} ($\sigma_{tr_pu} > \sigma_{min}$), the interface counter-slip length y is equal to interface debonded length L_d , i.e., $y(\sigma_{tr_pu}) = L_d$; upon reloading to σ_{tr_pr} ($\sigma_{tr_pr} < \sigma_{max}$), the interface new-slip length z is equal to interface debonded length L_d , i.e., $z(\sigma_{tr_pr}) = L_d$. When $\sigma_t < \sigma_{max} < \sigma_b$, the interface counter-slip length y and interface new-slip length z are less than interface debonded length L_d upon unloading to σ_{min} or reloading to σ_{max} , i.e., $y(\sigma_{min}) < L_d$ and $z(\sigma_{max}) < L_d$.

When $\sigma_b < \sigma_{max} < \sigma_p$, the interface completely debonds, and the interface counter-slip length y unloading to σ_{min} and interface new-slip length z upon reloading to σ_{max} , are both less than half matrix crack spacing $L/2$, i.e., $y(\sigma_{min}) < L/2$ and $z(\sigma_{max}) < L/2$. When $\sigma_p < \sigma_{max}$, the interface counter-slip length y and interface new-slip length z are affected by matrix cracking, i.e., upon unloading to σ_{tr_fu} ($\sigma_{tr_fu} > \sigma_{min}$), the interface counter-slip length y is equal to half matrix crack spacing $L/2$; Upon reloading to σ_{tr_fr} ($\sigma_{tr_fr} < \sigma_{max}$), the interface new-slip length z is equal to half matrix crack spacing $L/2$.

Based on the analysis of interface debonding and interface frictional slip between fibers and matrix corresponding to different peak stresses, the stress–strain hysteresis loops can be divided into four cases, i.e., (1) when $\sigma_{max} < \sigma_t$, the interface partially debonds, and fiber completely slips relative to matrix; (2) when $\sigma_t < \sigma_{max} < \sigma_b$, the interface partially debonds, and fiber partially slips relative to matrix; (3) when $\sigma_b < \sigma_{max} < \sigma_p$, the interface completely debonds, and fiber slips partially relative to matrix; (4) when $\sigma_p < \sigma_{max}$, the interface completely debonds, and fiber slips completely relative to matrix in the interface debonded region upon unloading/reloading.

For interface slip Case 2, the unloading and reloading stress–strain relationships for interface partially debonding and fiber partially slipping relative to matrix are,

$$\epsilon_{c_pu} = \frac{\sigma}{V_f E_f} + 4 \frac{\tau_i}{E_f} \frac{y^2}{r_f L} - 2 \frac{\tau_i (2y - L_d)(2y + L_d - L)}{E_f r_f L} - (\alpha_c - \alpha_f) \Delta T \tag{4a}$$

$$\begin{aligned} \epsilon_{c_pr} = & \frac{\sigma}{V_f E_f} - 4 \frac{\tau_i}{E_f} \frac{z^2}{r_f L} + 4 \frac{\tau_i (y - 2z)^2}{E_f r_f L} \\ & + 2 \frac{\tau_i (L_d - 2y + 2z)(L_d + 2y - 2z - L)}{E_f r_f L} - (\alpha_c - \alpha_f) \Delta T \end{aligned} \tag{4b}$$

where α_f , α_m and α_c denote the fiber, matrix and composite thermal expansion coefficient, respectively; and ΔT denotes the temperature difference between the fabricated temperature T_0 and room temperature T_1 ($\Delta T = T_1 - T_0$).

For interface slip Case 1, the unloading and reloading stress–strain relationships are divided into two regions. When $\sigma > \sigma_{tr_pu}$, the unloading strain is determined by Eq. 4a; and when $\sigma < \sigma_{tr_pu}$, the unloading strain is determined by Eq. 4a by setting $y = L_d$. When $\sigma < \sigma_{tr_pr}$, the reloading strain is determined by Eq. 4b; and when $\sigma > \sigma_{tr_pr}$, the reloading strain is determined by Eq. 4b by setting $z = L_d$.

For interface slip Case 3, the unloading and reloading stress–strain relationships for the interface completely debonding and fiber partially slipping relative to matrix are,

$$\epsilon_{c-fu} = \frac{\sigma}{V_f E_f} + 4 \frac{\tau_i}{E_f} \frac{y^2}{r_f L} - 2 \frac{\tau_i}{E_f} \frac{(2y-L/2)^2}{r_f L} - (\alpha_c - \alpha_f) \Delta T \tag{5a}$$

$$\begin{aligned} \epsilon_{c-fr} = & \frac{\sigma}{V_f E_f} - 4 \frac{\tau_i}{E_f} \frac{z^2}{r_f L} + 4 \frac{\tau_i}{E_f} \frac{(y-2z)^2}{r_f L} \\ & - 2 \frac{\tau_i}{E_f} \frac{(L/2 - 2y + 2z)^2}{r_f L} - (\alpha_c - \alpha_f) \Delta T \end{aligned} \tag{5b}$$

For interface slip Case 4, the unloading and reloading stress–strain relationships are divided into two regions. When $\sigma > \sigma_{tr_fu}$, the unloading strain is determined by Eq. 5a; and when $\sigma < \sigma_{tr_fu}$, the unloading strain is determined by Eq. 5a by setting $y=L/2$. When $\sigma < \sigma_{tr_fr}$, the reloading strain is determined by Eq. 5b; and when $\sigma > \sigma_{tr_fr}$, the reloading strain is determined by Eq. 5b by setting $z=L/2$.

Under fatigue loading, the area associated with the stress–strain hysteresis loops is the energy lost during corresponding cycle, which is defined as,

$$S = \int_{\sigma_{min}}^{\sigma_{max}} [\epsilon_c^{unload}(\sigma) - \epsilon_c^{reload}(\sigma)] d\sigma \tag{6}$$

The hysteresis loss energy of the four interface slip cases can be derived through inserting corresponding unloading and reloading strains into Eq. (6).

Under fatigue loading, the interface shear stress degrades with increase of the applied cycles due to interface wear at room temperature or interface oxidation at elevated temperature. The fatigue hysteresis loops, hysteresis loss energy and interface slip of unidirectional SiC/CAS composite under $\sigma_{max}=240$ MPa are shown in Fig. 1. The hysteresis loops corresponding to the 1st, 2nd, 3rd and 4th interface slip cases are illustrated in Fig. 1a. When $\tau_i=27\sim50$ MPa, i.e., the A–B part in Fig. 1b, the hysteresis loss energy increases with decrease of interface shear stress, and the hysteresis loops correspond to interface slip Case 1, i.e., the interface partially debonds, i.e., $L_d < L/2$ in Fig. 1c, and fiber completely slips relative to matrix in the interface debonded region, i.e., $y(\sigma_{min})=L_d$ in Fig. 1d. When $\tau_i=8.8\sim27$ MPa, i.e., the B–C part in Fig. 1b, the hysteresis loss energy increases with decrease of interface shear stress, and the hysteresis loops correspond to interface slip Case 2, i.e., the interface partially debonds, i.e., $L_d < L/2$ in Fig. 1c, and fiber partially slips relative to matrix in the interface debonded region, i.e., $y(\sigma_{min}) < L_d$ in Fig. 1d. When $\tau_i=8.3\sim8.8$ MPa, i.e., the C–D part in Fig. 1b, the hysteresis loss energy increases with decrease of interface shear stress and the hysteresis loops correspond to interface slip Case 3, i.e., the interface completely debonds, i.e., $L_d=L/2$ in Fig. 1c, and fiber partially slips relative to matrix in the interface debonded region, i.e., $y(\sigma_{min}) < L/2$ in Fig. 1d. When $\tau_i=1\sim8.3$ MPa, i.e., the D–E part in Fig. 1b, the hysteresis loss energy increases to the peak value, then decreases with decrease of interface shear stress, and the hysteresis loops correspond to interface slip Case 4, i.e., the interface completely debonds, i.e., $L_d=L/2$ in Fig. 1c, and fiber completely slips relative to matrix in the interface debonded region, i.e., $y(\sigma_{min})=L/2$ in Fig. 1d.

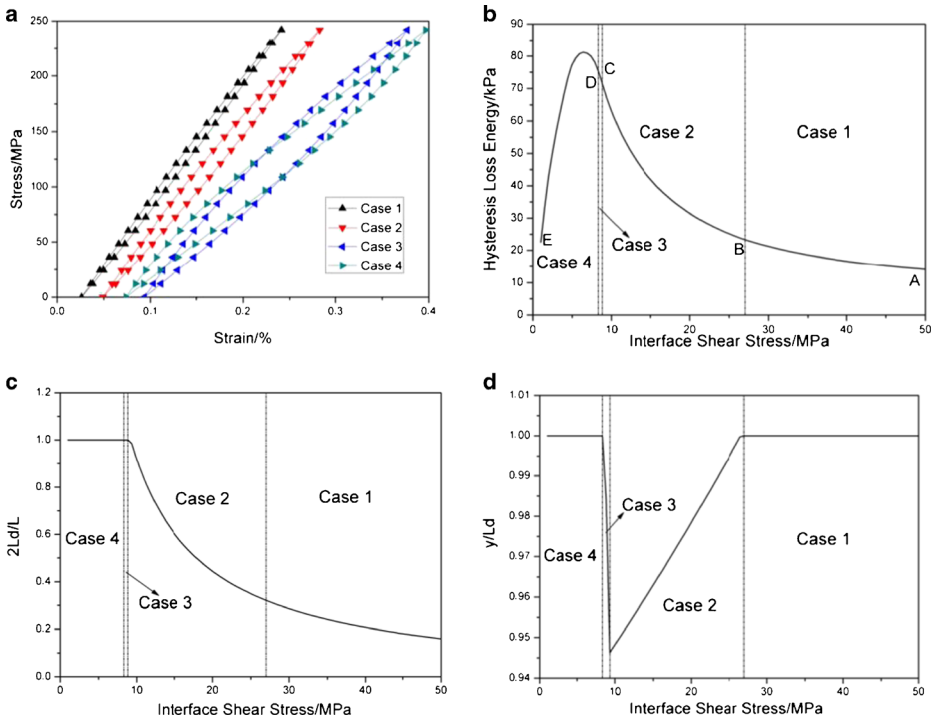


Fig. 1 **a** The fatigue hysteresis loops of four different interface slip cases; **b** the fatigue hysteresis loss energy versus interface shear stress; **c** the interface debonded length $2L_d/L$ versus interface shear stress; and **d** the interface counter-slip length y/L_d versus interface shear stress of unidirectional SiC/CAS composite under $\sigma_{\max} = 240$ MPa

The energy dissipation through relative slip between fibers and matrix in the interface debonded region would be affected by fatigue peak stress, fatigue stress amplitude, fiber volume fraction, matrix multicracking and cycle number. The relationships between hysteresis loss energy and interface shear stress corresponding to different fatigue peak stress, fatigue stress amplitude, fiber volume fraction and matrix crack spacing are shown in Fig. 2. With increase of the fatigue peak stress or fatigue stress amplitude, the range and extent of interface frictional slip between fibers and matrix in the interface debonded region would be increased, and the hysteresis loss energy would be increased at the same interface shear stress, as shown in Fig. 2a and b. With increase of the fiber volume fraction or matrix crack spacing, the range and extent of interface frictional slip between fibers and matrix in the interface debonded region would be decreased, and the hysteresis loss energy would be decreased at the same interface shear stress, as shown in Fig. 2c and d.

Under fatigue loading of cross-ply CMCs, transverse cracking in the 90° ply, matrix cracking and fiber/matrix interface debonding in the 0° ply would occur. Kuo and Chou [27] investigated the matrix multicracking in cross-ply CMCs and classified the cracking states into five modes, i.e., (1) transverse cracking; (2) transverse cracking and matrix cracking with perfect fiber/matrix interface bonding; (3) transverse cracking and matrix cracking with fiber/matrix interface debonding; (4) matrix cracking with perfect fiber/matrix interface bonding; and (5) matrix cracking with fiber/matrix interface debonding, as shown in Fig. 3. Among the matrix cracking modes, cracking mode 3 and mode 5

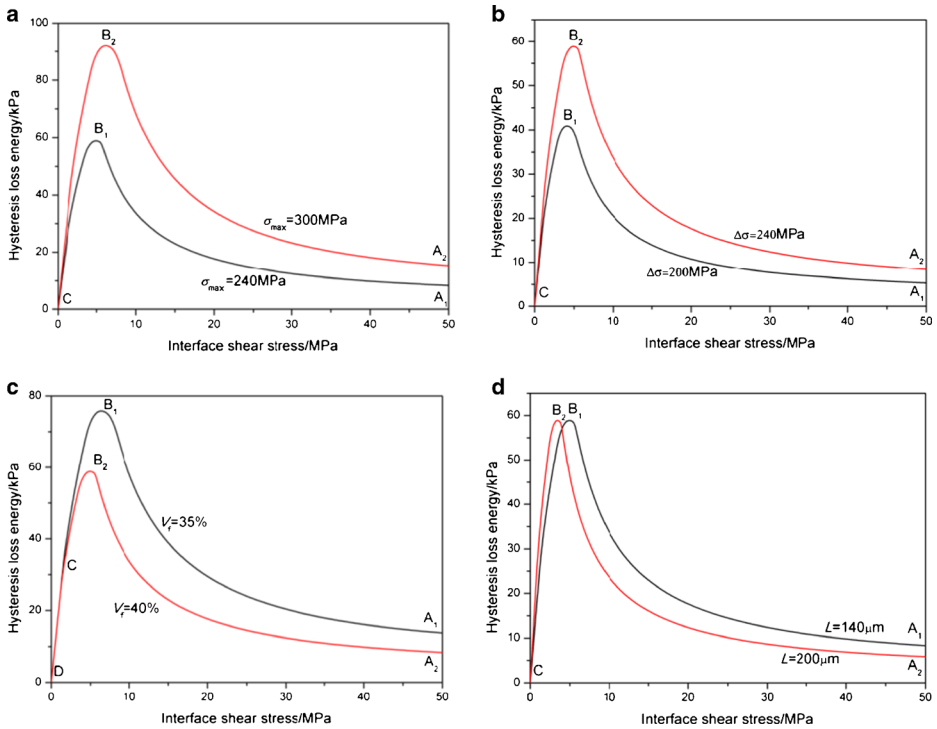


Fig. 2 The effects of **a** the fatigue peak stress; **b** the fatigue stress amplitude; **c** the fiber volume fraction; and **d** the matrix crack spacing on the evolution of fatigue hysteresis loss energy versus interface shear stress

involve matrix cracking and fiber/matrix interface debonding in the 0° ply. The relationships of the fatigue hysteresis loss energy and the interface shear stress for cracking mode 3 and mode 5 are shown in Fig. 4. At the same interface shear stress, the hysteresis loss energy of cracking mode 3 is much larger than that of cracking mode 5, i.e., A₁–B₁–C for cracking mode 3 and A₂–B₂–C for cracking mode 5 as shown in Fig. 4, which indicates that the extent of interface frictional slip between fibers and matrix of cracking mode 3 is much larger than that of cracking mode 5.

3 Experimental Analysis

When a CMC is subjected to a cyclic loading between a valley stress and a peak stress, upon first loading to the peak stress, the damage mechanisms of matrix multicroacking and fiber/matrix interface debonding would occur. Under subsequent cycles, interface shear stress degrades due to interface wear at room temperature or interface oxidation at elevated temperature. This should lead to the evolution of energy dissipated during a loading/unloading cycle. The evolution characteristics of hysteresis loss energy in different types of CMCs, i.e., unidirectional C/SiC, SiC/CAS, SiC/CAS–II and SiC/1723, cross-ply C/SiC, SiC/CAS, and SiC/MAS–L, 2D SiC/SiC, 2.5D C/SiC CMCs at room and elevated temperatures, would be investigated.

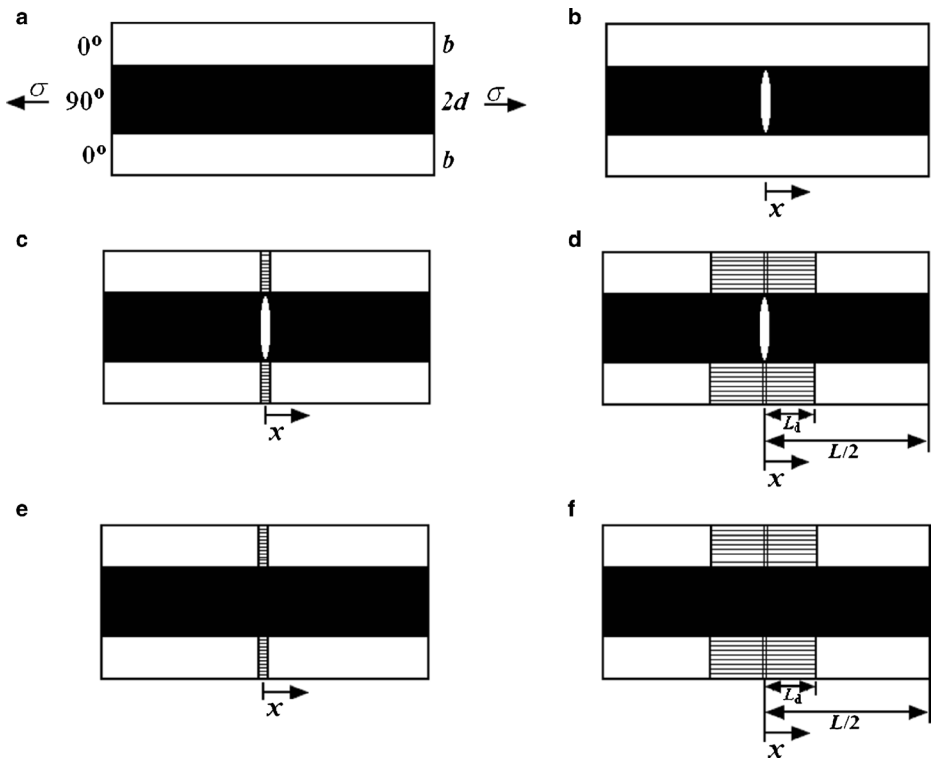


Fig. 3 The undamaged state and five damaged modes of cross-ply ceramic composite **a** undamaged composite; **b** mode 1: transverse cracking; **c** mode 2: transverse cracking and matrix cracking with perfect fiber/matrix bonding; **d** mode 3: transverse cracking and matrix cracking with fiber/matrix interface debonding; **e** mode 4: matrix cracking with perfect fiber/matrix bonding; and **f** mode 5: matrix cracking with fiber/matrix debonding

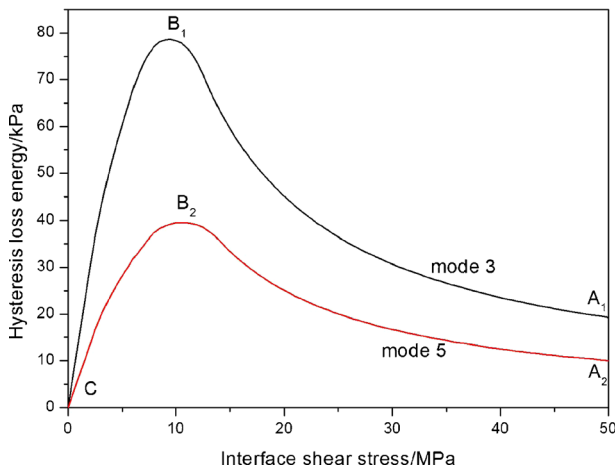


Fig. 4 The effect of matrix cracking mode, i.e., matrix cracking mode 3 and mode 5, on the fatigue hysteresis loss energy versus interface shear stress curve

3.1 Unidirectional CMCs

3.1.1 Room Temperature

The tension–tension fatigue behavior of unidirectional C/SiC composite has been investigated at room temperature. The fatigue experiments were in a sinusoidal wave form and a loading frequency of 10 Hz. The fatigue load ratio was 0.1, and the maximum number of applied cycles was defined to be 1,000,000 cycles. Under $\sigma_{\max}=240$ MPa, the experimental hysteresis loops corresponding to the 1st, 10th, 10000th, 100000th and 1000000th cycles are shown in Fig. 5a. The theoretical hysteresis loss energy versus interface shear stress curve is illustrated in Fig. 5b, in which the hysteresis loss energy increases with decrease of the interface shear stress to the peak value of 79.5 KPa (the corresponding interface shear stress is $\tau_i=4.7$ MPa), then decreases with decrease of interface shear stress to zero KPa (the corresponding interface shear stress is zero MPa).

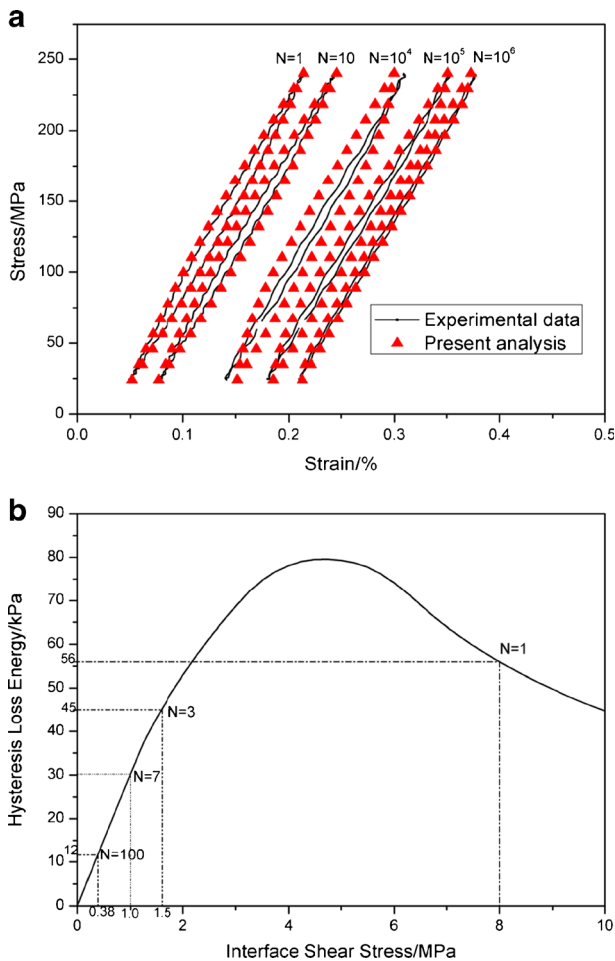


Fig. 5 a The experimental and predicted fatigue hysteresis loops; and b the theoretical fatigue hysteresis loss energy as a function of interface shear stress of unidirectional C/SiC composite under $\sigma_{\max}=240$ MPa at room temperature

shear stress is $\tau_i = \text{zero MPa}$). The experimental hysteresis loss energy of the 1st, 3rd, 7th, 10th, 100th, 1000th, 10000th and 100000th cycles are 56, 45, 30, 12.7, 12, 10.4, 8.8 and 8 KPa, respectively. Under $\sigma_{\max} = 240 \text{ MPa}$, the hysteresis loss energy of the first cycle lies in the right part of the hysteresis loss energy versus interface shear stress curve. The hysteresis loop of the first cycle corresponds to interface slip Case 2, i.e., the interface partially debonds and fiber partially slips relative to matrix in the interface debonded region upon unloading/reloading. When interface completely debonds, the interface shear stress degrades rapidly due to interface radial thermal residual tensile stress. The hysteresis loop of the 100th cycle corresponds to interface slip Case 4, i.e., the interface completely debonds and fiber completely slips relative to matrix in the interface debonded region upon unloading/reloading. The theoretical predicted hysteresis loops corresponding to the 1st, 10th, 1000th, 10000th, 100000th cycles agreed with experimental data, as shown in Fig. 5a.

Evans et al. [6] performed an investigation on the tension–tension fatigue behavior of unidirectional SiC/CAS composite at room temperature. The fatigue peak and valley stresses were 280 and 14 MPa, respectively. The fatigue loading was in a sinusoidal waveform and a frequency of 10 Hz. The fatigue tests were run out to 40,000 cycles or to fracture. The experimental hysteresis loops corresponding to the 1st, 5th, 9th, 109th and 30040th cycles are given in Fig. 6a. The theoretical hysteresis loss energy versus interface shear stress curve is illustrated in Fig. 6b, in which the hysteresis loss energy increases with decrease of the interface shear stress to the peak value of 81 KPa (the corresponding interface shear stress is $\tau_i = 7 \text{ MPa}$), then decreases to zero KPa with decrease of interface shear stress. Under $\sigma_{\max} = 280 \text{ MPa}$, the experimental hysteresis loss energy increases first, then decreases with increase of the number of applied cycles, corresponding to the right and left parts of the hysteresis loss energy versus interface shear stress curve. The predicted hysteresis loops corresponding to the 1st, 5th, 9th, 109th and 30040th cycles agreed with experimental data, as shown in Fig. 6a.

Holmes and Cho [10] investigated the tension–tension fatigue behavior of unidirectional SiC/CAS–II composite at room temperature. The fatigue loading was performed under load control using a sinusoidal waveform and a frequency of 25 Hz. The fatigue peak and valley stresses were 180 and 10 MPa, respectively. The specimen failure occurred at approximately 3.21×10^6 cycles. The hysteresis loops corresponding to the 3rd, 10th, 20th and 3200th cycles are shown in Fig. 7a. The theoretical hysteresis loss energy versus interface shear stress curve is illustrated in Fig. 7b, in which the hysteresis loss energy increases with decrease of the interface shear stress to the peak value of 42.6 KPa (the corresponding interface shear stress is $\tau_i = 3.4 \text{ MPa}$), then decreases with decrease of the interface shear stress to zero KPa (the corresponding interface shear stress is $\tau_i = \text{zero MPa}$). The experimental hysteresis loss energy of the 3rd, 10th, 20th and 3200th cycles are 5, 9, 16 and 25 KPa, respectively. Under $\sigma_{\max} = 180 \text{ MPa}$, the hysteresis loss energy increases with increase of the number of applied cycles, corresponding to the right part of the hysteresis loss energy versus interface shear stress curve. The predicted hysteresis loops corresponding to the 3rd, 10th, 20th and 3200th cycles agreed with experimental data, as shown in Fig. 7a.

Zawada et al. [28] investigated the tension–tension fatigue behavior of unidirectional SiC/1723 composite at room temperature. The fatigue tests were conducted under load control and a stress ratio of 0.1 and sinusoidal frequency of 10 Hz. The fatigue peak and valley stresses were 500 and 50 MPa, respectively. The fatigue tests were allowed to run for up to 1,000,000 cycles, after which the tests were terminated. The hysteresis loops corresponding to the 10th, 20th, 143th, 1010th and 10011th cycles are shown in Fig. 8a. The theoretical hysteresis loss energy versus interface shear stress curve is illustrated in Fig. 8b, in which the hysteresis loss energy increases with decrease of the interface shear stress to the peak value of 160 KPa (the corresponding interface shear stress is

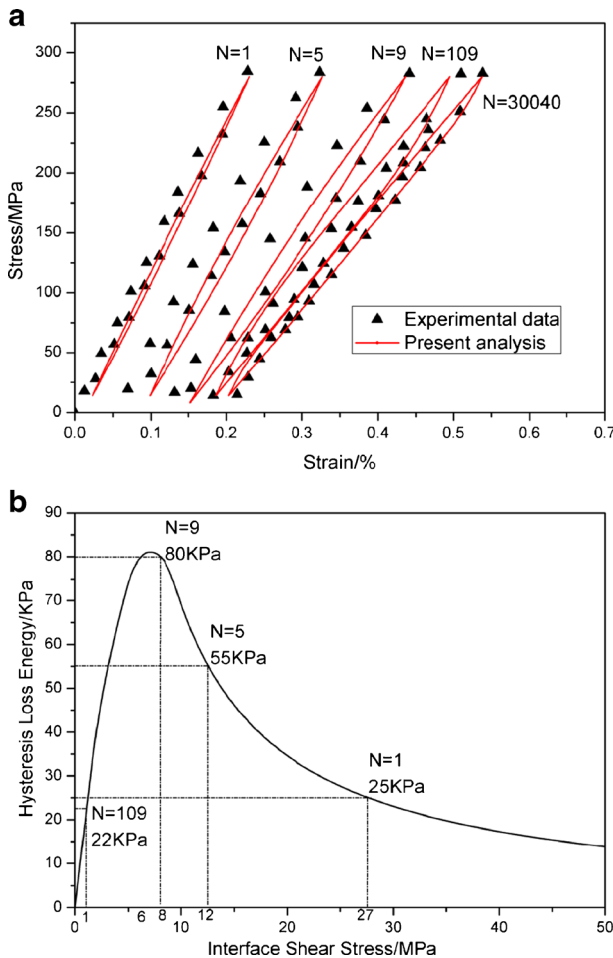


Fig. 6 a The fatigue hysteresis loops of different number of applied cycles; and b the fatigue hysteresis loss energy versus interface shear stress of unidirectional SiC/CAS composite under $\sigma_{max}=280$ MPa at room temperature

$\tau_i=4.2$ MPa), then decreases with decrease of the interface shear stress to zero KPa (the corresponding interface shear stress is $\tau_i =$ zero MPa). The experimental hysteresis loss energy of the 10th, 20th, 143th 1010th and 10011th cycles are 25, 25, 26, 27 and 38 KPa, respectively. Under $\sigma_{max}=500$ MPa, the hysteresis loss energy increases with increase of the number of applied cycles, corresponding to the right part of the hysteresis loss energy versus interface shear stress curve. The predicted hysteresis loops corresponding to the 10th, 20th, 143th 1010th and 10011th cycles agreed with experimental data, as shown in Fig. 8a.

3.1.2 Elevated Temperature

The tension–tension fatigue behavior of unidirectional C/SiC composite has been investigated at 800 °C in air atmosphere. The fatigue experiments were in a sinusoidal wave form and a loading frequency of 10 Hz. The fatigue load ratio was 0.1, and the maximum number of

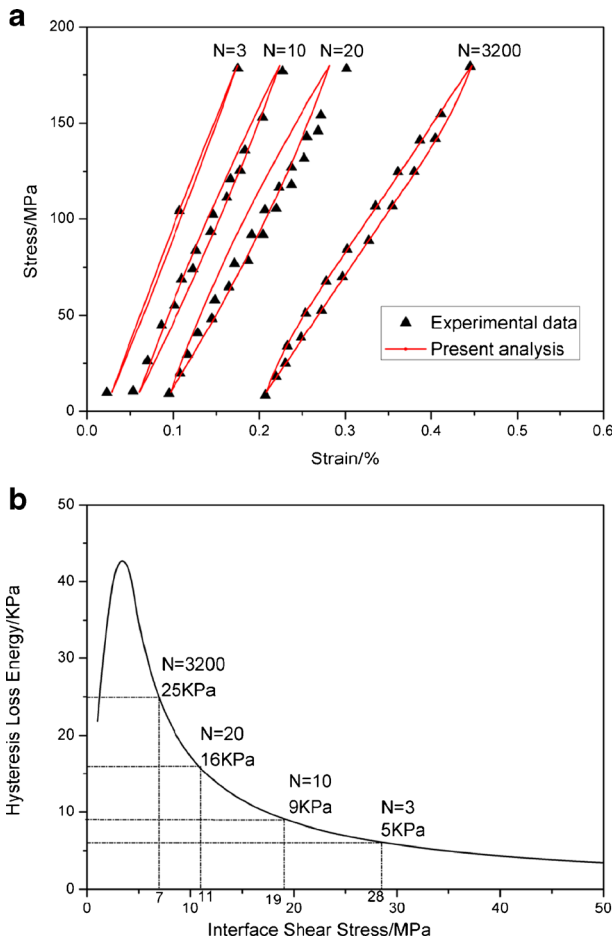


Fig. 7 **a** The fatigue hysteresis loops of different number of applied cycles; and **b** the fatigue hysteresis loss energy versus interface shear stress of unidirectional SiC/CAS-II composite under $\sigma_{\max}=180$ MPa at room temperature

applied cycles was defined to be 1,000,000 cycles. Under $\sigma_{\max}=250$ MPa, the experimental hysteresis loops corresponding to the 1st, 1000th, 5000th, 10000th, 15000th, 20000th and 24000th cycles are shown in Fig. 9a. The theoretical hysteresis loss energy versus interface shear stress curve is illustrated in Fig. 9b, in which the hysteresis loss energy increases with decrease of the interface shear stress to the peak value of 90 KPa (the corresponding interface shear stress is $\tau_i=4.8$ MPa), then decreases with decrease of the interface shear stress to zero KPa (the corresponding interface shear stress is $\tau_i =$ zero MPa). The experimental hysteresis loss energy of the 1st, 100th, 1000th, 5000th, 10000th, 15000th, 20000th and 24000th cycles are 62, 50, 24, 16, 12, 8, 7.8 and 7.2 KPa, respectively. Under $\sigma_{\max}=250$ MPa, the hysteresis loss energy of the first cycle lies in the right part of the hysteresis loss energy versus interface shear stress curve. The hysteresis loop of the first cycle corresponds to interface slip Case 2, i.e., the interface partially debonds and fiber partially slips relative to matrix in the interface debonded region upon unloading/reloading. When interface completely debonds, the interface

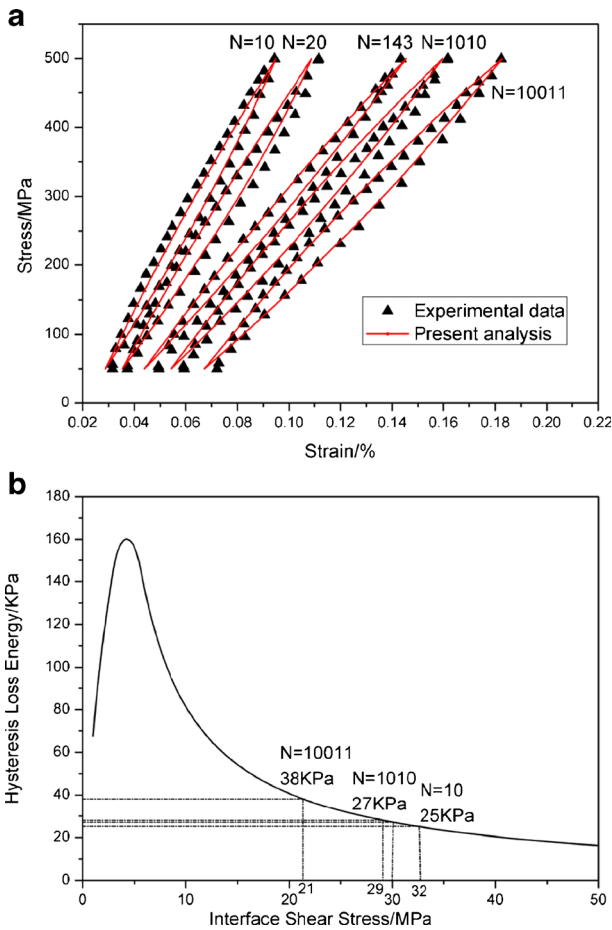


Fig. 8 **a** The fatigue hysteresis loops of different number of applied cycles; and **b** the fatigue hysteresis loss energy versus interface shear stress of unidirectional SiC/1723 composite under $\sigma_{max}=500$ MPa at room temperature

shear stress degrades rapidly due to interface radial thermal residual tensile stress. The hysteresis loop of the 100th cycle corresponds to interface slip Case 4, i.e., the interface completely debonds and fiber completely slips relative to matrix in the interface deboned region upon unloading/reloading. The predicted hysteresis loops corresponding to the 1st, 1000th, 5000th, 10000th, 15000th, 20000th and 24000th cycles agreed with experimental data, as shown in Fig. 9a.

3.2 Cross-Ply CMCs

3.2.1 Room Temperature

The tension–tension fatigue behavior of cross-ply C/SiC composite has been investigated at room temperature. The fatigue experiments were in a sinusoidal wave form and a loading frequency of 10 Hz. The fatigue load ratio was 0.1, and the maximum number of applied

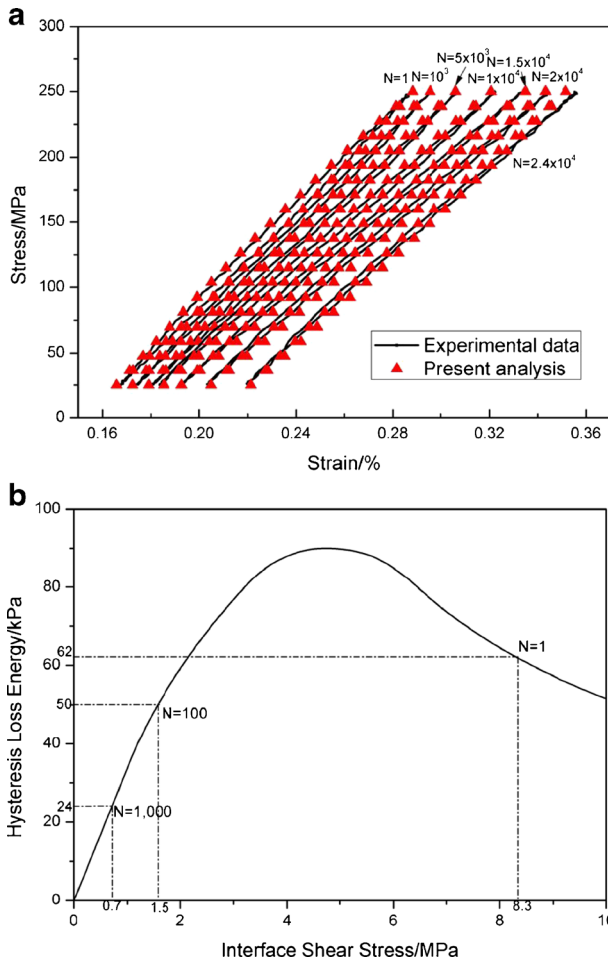


Fig. 9 **a** The experimental and predicted fatigue hysteresis loops; and **b** the theoretical fatigue hysteresis loss energy as a function of interface shear stress of unidirectional C/SiC composite under $\sigma_{max}=250$ MPa at 800 °C in air atmosphere

cycles was defined to be 1,000,000 cycles. Under $\sigma_{max}=105$ MPa, the hysteresis loops corresponding to the 4000th, 10000th, 100000th and 1000000th cycles are shown in Fig. 10a. The theoretical hysteresis loss energy versus interface shear stress curve is illustrated in Fig. 10b, in which the hysteresis loss energy increases with decrease of interface shear stress to the peak value of 36.4 KPa (the corresponding interface shear stress is $\tau_i=6.1$ MPa), then decreases with decrease of the interface shear stress to zero KPa (the corresponding interface shear stress is $\tau_i =$ zero MPa). The experimental hysteresis loss energy of the 1st, 3rd, 5th, 7th, 100th, 1000th, 4000th, 10000th, 100000th and 1000000th cycles are 35, 32, 28, 26, 21.5, 19.4, 18.2, 16.9, 12.8 and 10.7 KPa, respectively. Under $\sigma_{max}=105$ MPa, the hysteresis loss energy of the first cycle lies in the right part of the hysteresis loss energy versus interface shear stress curve. The hysteresis loop of the first cycle corresponds to interface slip Case 2, i.e., the interface partially debonds and fiber partially slips relative to matrix in the interface debonded region upon unloading/reloading. The hysteresis loop of the 100th cycle corresponds to

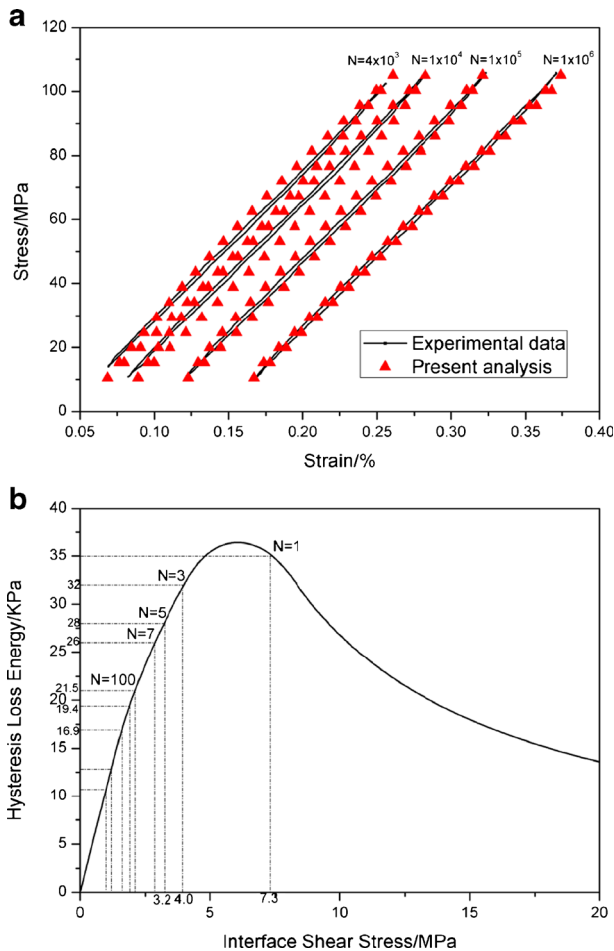


Fig. 10 a The experimental and predicted fatigue hysteresis loops; and b the theoretical fatigue hysteresis loss energy as a function of interface shear stress in the 0° ply of cross-ply C/SiC composite under $\sigma_{\max}=105$ MPa at room temperature

interface slip Case 4, i.e., the interface completely debonds and fiber completely slips relative to matrix in the interface debonded region upon unloading/reloading. The predicted hysteresis loops corresponding to the 4000th, 10000th, 100000th and 1000000th cycles agreed with experimental data, as shown in Fig. 10a.

Opalski et al. [29] investigated the tension–tension fatigue behavior of cross-ply SiC/CAS composite at room temperature. The fatigue loading was in a sinusoidal waveform and a frequency of 10 Hz. The fatigue peak and valley stresses were 180 and 18 MPa, respectively. The fatigue tests were run either until the specimen failed or 1000000 cycles were achieved. The hysteresis loops corresponding to the 10th, 100th and 1000th cycles are shown in Fig. 11a. The theoretical hysteresis loss energy versus interface shear stress curve is illustrated in Fig. 11b in which the hysteresis loss energy increases with decrease of interface shear stress to the peak value of 62.8 KPa (the corresponding interface shear stress is $\tau_i=9.8$ MPa), then decreases with decrease of the interface shear stress to zero KPa (the corresponding interface

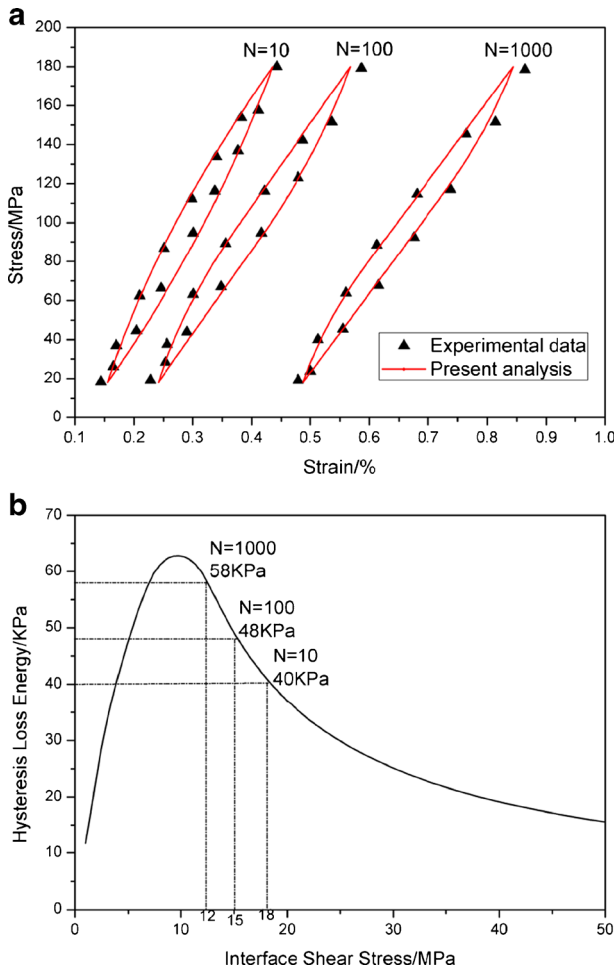


Fig. 11 **a** The fatigue hysteresis loops of different number of applied cycles; and **b** the fatigue hysteresis loss energy versus interface shear stress in the 0° ply of cross-ply SiC/CAS composite under $\sigma_{\max}=180$ MPa at room temperature

shear stress is $\tau_1 =$ zero MPa). The experimental hysteresis loss energy of the 10th, 100th and 1000th cycles are 40, 48 and 58 KPa, respectively. Under $\sigma_{\max}=180$ MPa, the hysteresis loss energy increases with increase of the number of applied cycles, corresponding to the right part of the hysteresis loss energy versus interface shear stress curve. The increase of the hysteresis loss energy is attributed to degradation of interface shear stress and the increase of interface debonded region. The theoretical predicted hysteresis loops corresponding to the 10th, 100th and 1000th cycles agreed with experimental data, as shown in Fig. 11a.

3.2.2 Elevated Temperature

The tension–tension fatigue behavior of cross-ply C/SiC composite has been investigated at 800°C in air atmosphere. The fatigue experiments were in a sinusoidal wave form and a loading frequency of 10 Hz. The fatigue load ratio was 0.1, and the maximum number of

applied cycles was defined to be 1000000 cycles. Under $\sigma_{max}=105$ MPa, the hysteresis loops of the 4th, 10th, 100th, 500th, 1000th and 6000th cycles are given in Fig. 12a. The theoretical hysteresis loss energy versus interface shear stress curve is illustrated in Fig. 12b, in which the hysteresis loss energy increases with decrease of interface shear stress to the peak value of 25.6 KPa (the corresponding interface shear stress is $\tau_i=4.4$ MPa), then decreases with decrease of the interface shear stress to zero KPa (the corresponding interface shear stress is $\tau_i =$ zero MPa). The experimental hysteresis loss energy of the 1st, 2nd, 3rd, 4th, 10th, 100th, 500th, 1000th, 3000th, 6000th and 6600th cycles are 24.3, 20, 13, 12, 9.7, 8.6, 7.1, 6.1, 5.4, 5.2 and 5.1 KPa, respectively. Under $\sigma_{max}=105$ MPa, the hysteresis loss energy of the first cycle lies in the right part of the hysteresis loss energy versus interface shear stress curve. The hysteresis loop of the first cycle corresponds to interface slip Case 2, i.e., the interface partially debonds and fiber partially slips relative to matrix in the interface debonded region upon unloading/reloading. The hysteresis loop of the 100th cycle corresponds to interface slip Case

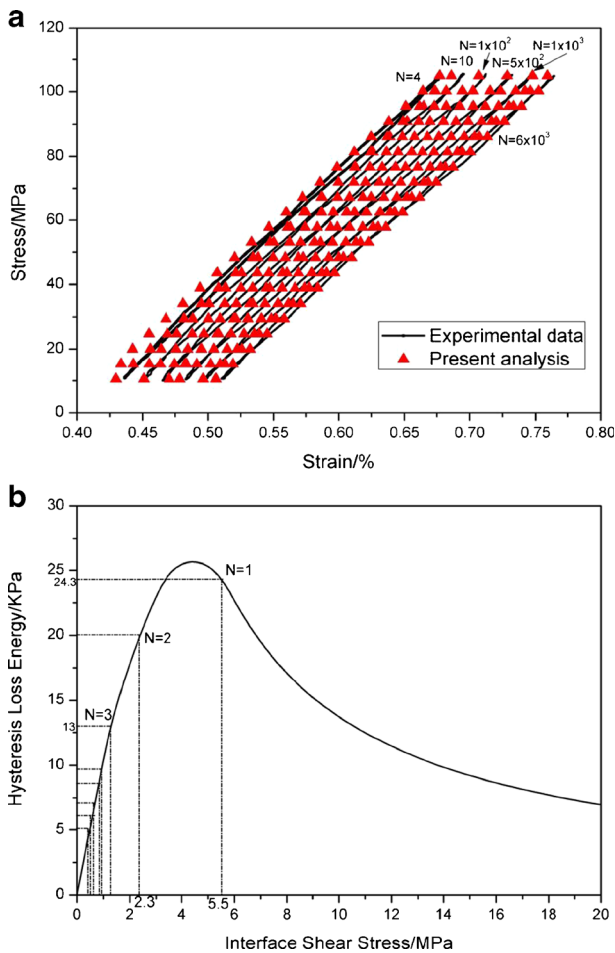


Fig. 12 **a** The experimental and predicted fatigue hysteresis loops; and **b** the theoretical fatigue hysteresis loss energy as a function of interface shear stress in the 0° ply of cross-ply C/SiC composite under $\sigma_{max}=105$ MPa at 800°C in air atmosphere

4, i.e., the interface completely debonds and fiber completely slips relative to matrix in the interface debonded region upon unloading/reloading. The theoretical predicted hysteresis loops corresponding to the 4th, 10th, 100th, 500th, 1000th and 6000th cycles agreed with experimental data, as shown in Fig. 12a.

Reynaud [12] investigated the tension–tension fatigue behavior of cross-ply SiC/MAS–L composite at 800 and 1000 °C in inert atmosphere. The fatigue loading frequency was 1 Hz. The fatigue peak and valley stresses were 110 and zero MPa, respectively. The hysteresis loops corresponding to each cycle have been recorded and analyzed. The experimental hysteresis loss energy versus the number of applied cycles curves are shown in Fig. 13a. The theoretical hysteresis loss energy versus interface shear stress curve is shown in Fig. 13b, in which the hysteresis loss energy increases with decrease of interface shear stress to the peak value of 19 KPa (the corresponding interface shear stress is $\tau_i=5.6$ MPa), then decreases with decrease

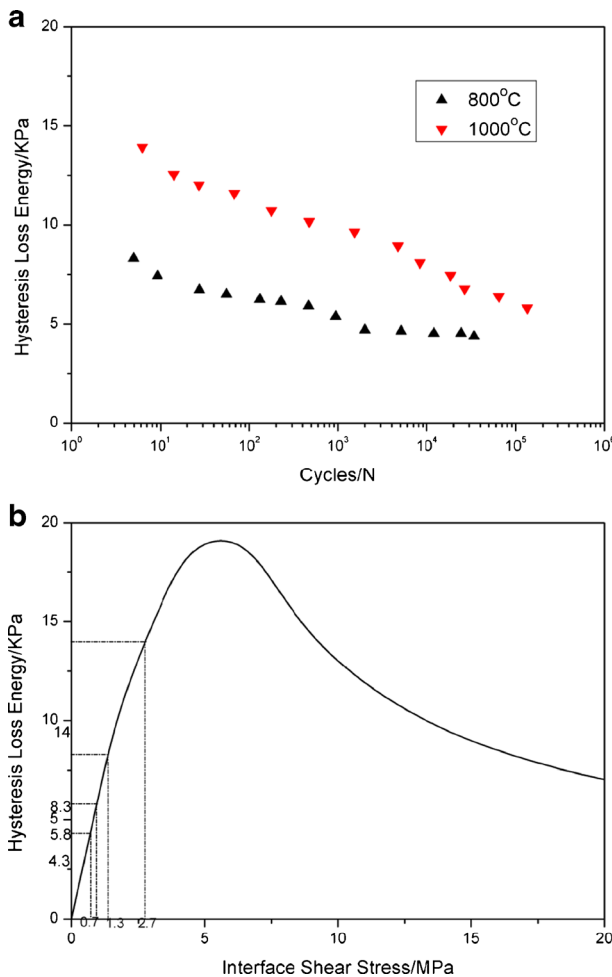


Fig. 13 **a** The fatigue hysteresis loss energy versus the number of applied cycles; and **b** the fatigue hysteresis loss energy versus interface shear stress in the 0° ply of cross-ply SiC/MAS–L composite under $\sigma_{\max}=110$ MPa at 800 and 1000 °C in inert atmosphere

of interface shear stress to zero KPa (the corresponding interface shear stress is $\tau_i = \text{zero MPa}$). At 800 °C in inert atmosphere, the experimental hysteresis loss energy degrades from 8.3 KPa at the 5th cycle to 4.3 KPa at the 34162th cycle; and at 1000 °C in inert atmosphere, the experimental hysteresis loss energy degrades from 14 KPa at the 6th cycle to 5.8 KPa at the 133925th cycle. As the radial thermal expansive coefficient of MAS–L matrix is lower than that of SiC fiber, the thermal residual tensile stress exists in the fiber/matrix interface, which lowers the interface shear stress. When the composite was cooled down from high fabricated temperature to room temperature, the fiber/matrix interface debonds. The radial thermal residual tensile stress decreases with increase of the test temperature, leading to the increase of interface shear stress with increase of test temperature. Under fatigue loading at elevated temperature, the hysteresis loss energy decreases with increase of the number of applied cycles, corresponding to the left part of the hysteresis loss energy versus interface shear stress curve. The hysteresis loops correspond to interface slip Case 4, i.e., the interface completely debonds and fiber completely slips relative to matrix in the interface debonded region upon unloading/reloading.

3.3 2D and 2.5D Woven CMCs

3.3.1 Room Temperature

Yang [30] investigated the tension–tension fatigue behavior of 2.5D C/SiC composite at room temperature. The fatigue loading was in a sinusoidal waveform and a frequency of 10 Hz. The tensile fatigue stress ratio was 0.1, and the maximum number of applied cycles was defined to be 1000000 cycles. The fatigue peak and valley stresses were 180 and 18 MPa, respectively. Under $\sigma_{\max} = 180$ MPa, the hysteresis loops corresponding to the 10th, 1010th, 4010th and 5210th cycles are shown in Fig. 14a. The specimen experienced 5281 cycles, then fatigue fractured. The theoretical hysteresis loss energy versus interface shear stress curve is illustrated in Fig. 14b, in which the hysteresis loss energy increases with decrease of the interface shear stress to the peak value of 35.8 KPa (the corresponding interface shear stress is $\tau_i = 2.4$ MPa), then decreases with decrease of the interface shear stress to zero KPa (the corresponding interface shear stress is $\tau_i = \text{zero MPa}$). The experimental hysteresis loss energy of the 10th, 1010th, 4010th and 5210th cycles are 7.8, 8.5, 9.4 and 12.8 KPa, respectively. Under $\sigma_{\max} = 180$ MPa, the hysteresis loss energy increases with increase of the number of applied cycles. The hysteresis loops from the first cycle to 5210th cycle all correspond to interface slip Case 2, i.e., the interface partially debonds and fiber partially slips relative to matrix in the interface debonded region upon unloading/reloading. The predicted hysteresis loops corresponding to the 10th, 1010th, 4010th and 5210th cycles agreed with experimental data, as shown in Fig. 14a.

3.3.2 Elevated Temperature

Yang [30] investigated the tension–tension fatigue behavior of 2.5D C/SiC composite at 800 °C in air atmosphere. The fatigue loading was in a sinusoidal waveform and a frequency of 10 Hz. The tensile fatigue stress ratio was 0.1, and the maximum number of applied cycles was defined to be 1000000 cycles. Under $\sigma_{\max} = 140$ MPa, the hysteresis loops of the 500th, 1500th, 2000th and 22700th cycles are shown in Fig. 15a. The specimen experienced 5281 cycles, then fatigue fractured. The theoretical hysteresis loss energy versus interface shear stress curve is shown in Fig. 15b, in which the hysteresis loss energy increases with

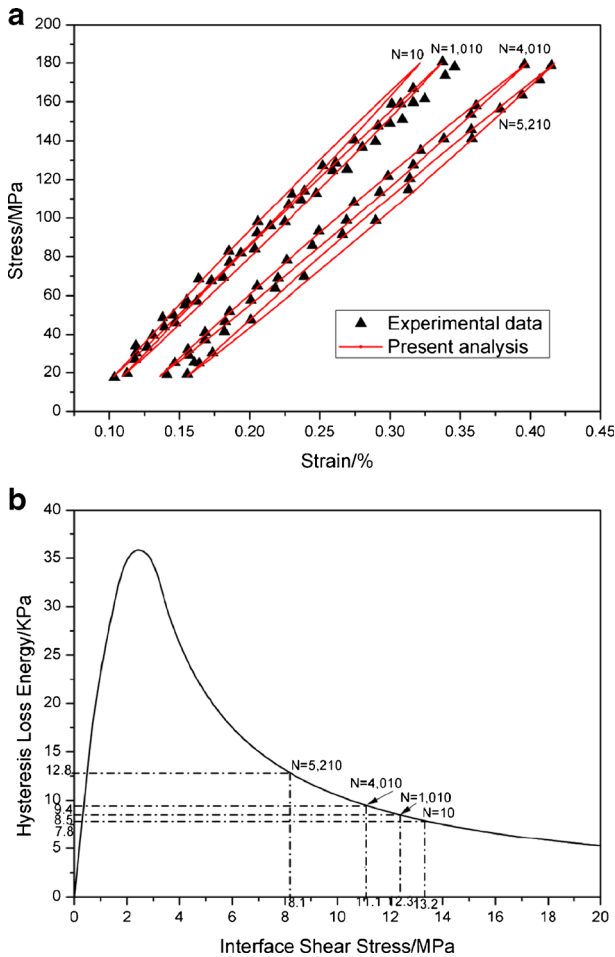


Fig. 14 **a** The experimental and predicted fatigue hysteresis loops; and **b** the theoretical fatigue hysteresis loss energy as a function of interface shear stress in the longitudinal yarns of 2.5D C/SiC composite under $\sigma_{max}=180$ MPa at room temperature

decrease of the interface shear stress to the peak value of 21.7 KPa (the corresponding interface shear stress is $\tau_i=2.25$ MPa), then decreases with decrease of interface shear stress to zero KPa (the corresponding interface shear stress is $\tau_i =$ zero MPa). The experimental hysteresis loss energy of the 500th, 15000th, 20000th and 22700th cycles are 6.3, 7.2, 8.7 and 11.8 KPa, respectively. Under $\sigma_{max}=140$ MPa, the hysteresis loss energy increases with increase of the number of applied cycles. The hysteresis loops from the 500th cycle to 22700th cycle all correspond to interface slip Case 2, i.e., the interface partially debonds and fiber partially slips relative to matrix in the interface debonded region upon unloading/reloading. The predicted hysteresis loops corresponding to the 500th, 15000th, 20000th and 22700th cycles agreed with experimental data, as shown in Fig. 15a.

Reynaud [12] investigated the tension–tension fatigue behavior of 2D SiC/SiC composite at 600, 800 and 1000 °C in inert atmosphere. The fatigue loading frequency was 1 Hz. The fatigue peak and valley stresses were 130 and zero MPa, respectively. The experimental

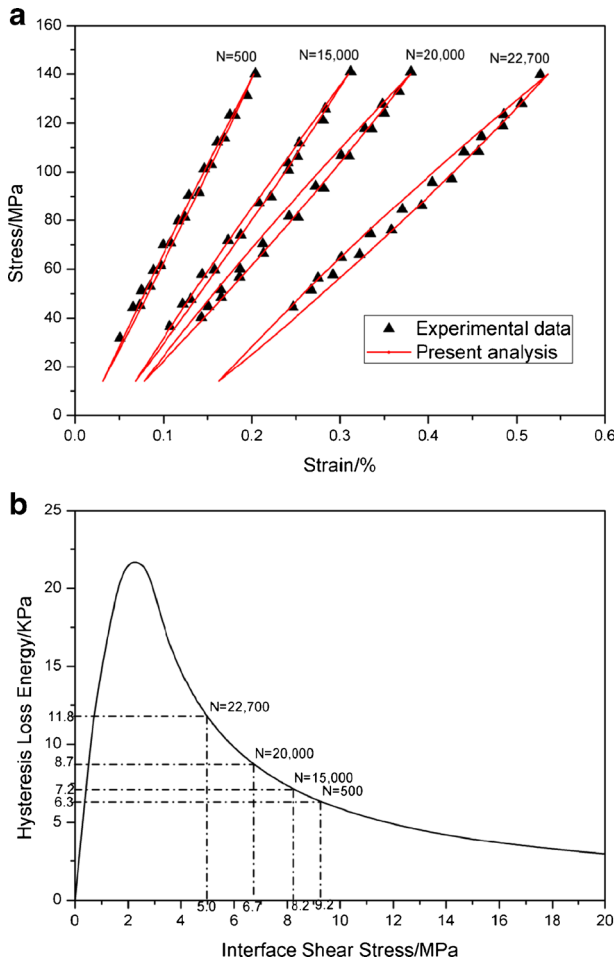


Fig. 15 **a** The experimental and predicted fatigue hysteresis loops; **b** the theoretical fatigue hysteresis loss energy as a function of interface shear stress in the longitudinal yarns of 2.5D C/SiC composite under $\sigma_{max} = 140$ MPa at 800 °C in air atmosphere

hysteresis loss energy versus the number of applied cycles curves are shown in Fig. 16a. At 600 °C in inert atmosphere, the hysteresis loss energy increases from 5.2 KPa at the 15th cycle to 9.4 KPa at the 333507th cycle; at 800 °C in inert atmosphere, the hysteresis loss energy increases from 9 KPa at the 23th cycle to 15.3 KPa at the 97894th cycle; and at 1000 °C in inert atmosphere, the hysteresis loss energy increases from 10 KPa at the 22th cycle to 21.8 KPa at the 117055th cycle. The theoretical hysteresis loss energy versus interface shear stress curve is illustrated in Fig. 16b. As the radial thermal expansive coefficient of SiC matrix is higher than that of SiC fiber, the radial thermal residual compressive stress exists in the fiber/matrix interface, which increases the interface shear stress. When the composite was cooled down from high fabricated temperature to room temperature, the radial thermal residual compressive stress and interface shear stress both decrease with increase of test temperature. Under fatigue loading at elevated temperature, the hysteresis loss energy increases with increase of the number of applied cycles, corresponding to the right part of the hysteresis loss

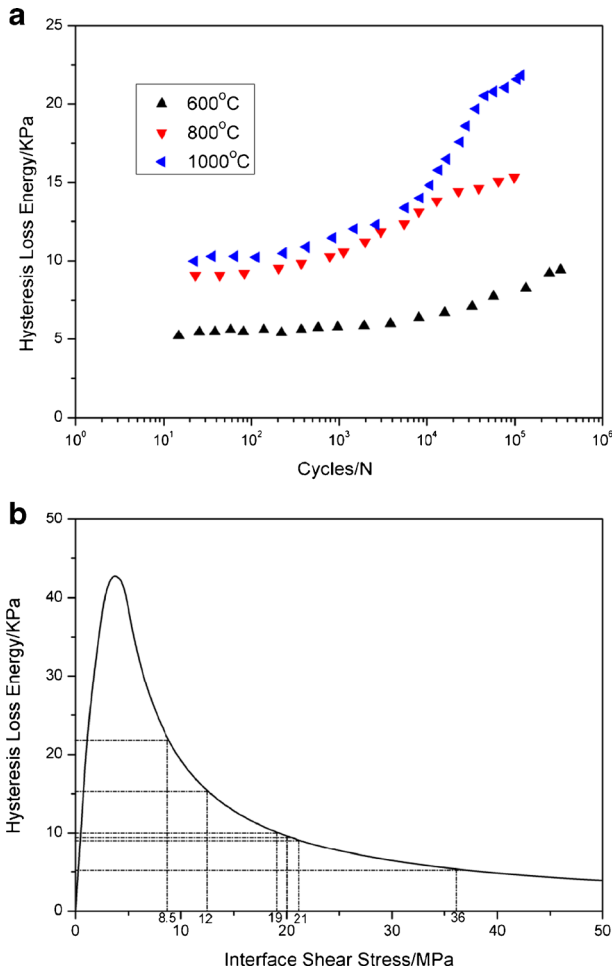


Fig. 16 **a** The fatigue hysteresis loss energy versus the number of applied cycles; and **b** the fatigue hysteresis loss energy versus interface shear stress in the longitudinal yarns of 2D SiC/SiC composite under $\sigma_{\max} = 130$ MPa at 600, 800 and 1000 °C in inert atmosphere

energy versus interface shear stress curve. The hysteresis loops correspond to interface slip Case 2, i.e., the interface partially debonds and fiber partially slips relative to matrix in the interface debonded region upon unloading/reloading.

Dalmaz et al. [31] investigated the tension–tension fatigue behavior of 2.5D C/SiC composite at 600 °C in inert atmosphere. The fatigue peak and valley stresses were 230 and zero MPa. The fatigue loading frequency was 1 Hz. The experimental hysteresis loops corresponding to the 10th, 100000th and 1000000th cycles are shown in Fig. 17a. The theoretical hysteresis loss energy versus interface shear stress curve is illustrated in Fig. 17b. As the axial thermal expansion coefficient of carbon fiber is lower than that of SiC matrix, the axial thermal residual tensile stress exists in the fiber/matrix interface, leading to microcracking in SiC matrix upon cooled down from high fabricated temperature to room temperature. The radial thermal expansion coefficient of carbon fiber is higher than that of SiC matrix, the radial thermal residual tensile stress exists in fiber/matrix interface, leading to interface debonding

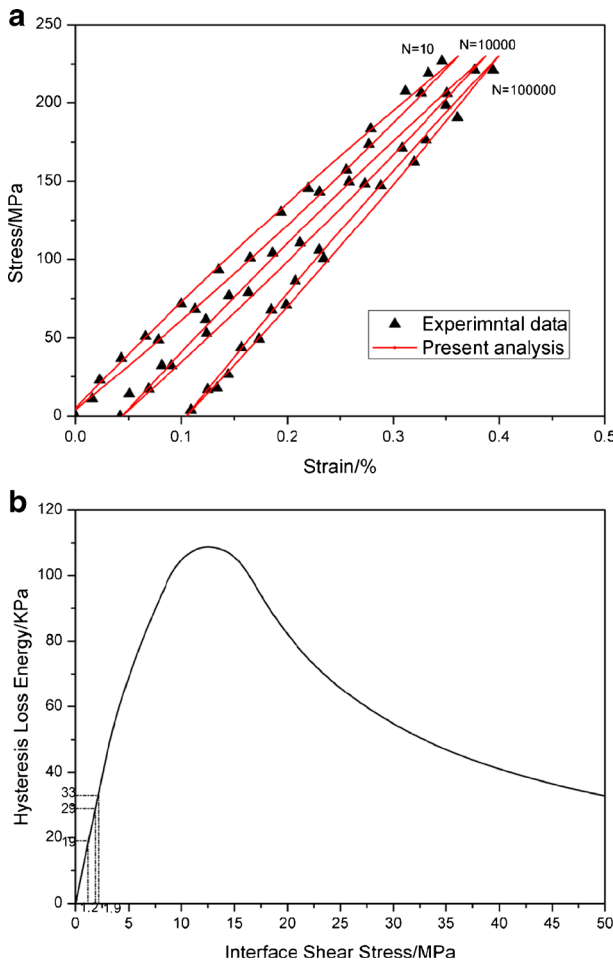


Fig. 17 **a** The fatigue hysteresis loops of different number of applied cycles; and **b** the fatigue hysteresis loss energy versus interface shear stress in the longitudinal yarns of 2.5D C/SiC composite under $\sigma_{max}=230$ MPa at 600 °C in inert atmosphere

upon cooled down from high fabrication temperature to room temperature. The experimental hysteresis loss energy of the 10th, 10000th and 100000th cycles are 33, 29 and 19 KPa, respectively. Under $\sigma_{max}=230$ MPa, the hysteresis loss energy decreases with increase of the number of applied cycles, corresponding to the left part of the hysteresis loss energy versus interface shear stress curve. The hysteresis loops correspond to interface slip Case 4, i.e., the interface completely debonds and fiber completely slips relative to matrix in the interface debonded region upon unloading/reloading. The predicted hysteresis loops corresponding to the 10th, 10000th and 100000th cycles agreed with experimental data, as shown in Fig. 17a.

3.4 Evolution Characteristic of Fatigue Hysteresis Loss Energy

The evolution characteristic of hysteresis loss energy under cyclic loading is not classical as usually the energy dissipated increases during fatigue as far as the material is damaged.

However, a general phenomenon occurring during cyclic fatigue is the decrease of fiber/matrix interface shear stress, due to interface wear at room temperature, i.e., to-and-fro slipping of fibers in the matrix near a matrix cracking, or interface oxidation at elevated temperature, i.e., the interphase oxidation with production of gaseous species of CO or CO₂.

For unidirectional and cross-ply C/SiC composites, the evolution of fatigue hysteresis loss energy with increase of applied cycles depends upon fatigue peak stress, fiber preform and test environment, i.e., under $\sigma_{\max}=240$ MPa at room temperature, the fatigue hysteresis loss energy of unidirectional C/SiC composite decreases from 56 KPa at the 1st cycle to 8 KPa at the 100000th cycle, the interface slip of the first cycle corresponds to Case 2; under $\sigma_{\max}=250$ MPa at 800 °C in air atmosphere, the fatigue hysteresis loss energy of unidirectional C/SiC composite decreases from 62 KPa at the first cycle to 7.2 KPa at the 24000th cycle, the interface slip of the first cycle corresponds to Case 2; under $\sigma_{\max}=105$ MPa, the fatigue hysteresis loss energy of cross-ply C/SiC composite decreases from 35 KPa at the first cycle to 10.7 KPa at the 100000th cycle at room temperature, and from 24.3 KPa at the first cycle to 5.1 KPa at the 6600th cycle at 800 °C in air atmosphere, the interface slip of the first cycle corresponds to Case 2. For 2.5D C/SiC composite, the evolution characteristics of fatigue hysteresis loss energy are different corresponding to different fatigue peak stresses and test conditions, i.e., under $\sigma_{\max}=180$ and 140 MPa at room temperature and 800 °C in air atmosphere, the fatigue hysteresis loss energy increases with increase of the applied cycles, from 7.8 KPa at the 10th cycle to 12.8 KPa at the 5210th cycle at room temperature, and from 6.3 KPa at the 500th cycle to 11.8 KPa at the 227000th cycle at 800 °C in air atmosphere; and under 230 MPa at 600 °C in inert atmosphere, the fatigue hysteresis loss energy decreases with increase of the applied cycles, from 33 KPa at the 10th cycle to 19 KPa at the 100000th cycle.

For unidirectional SiC/CAS, SiC/CAS-II and SiC/1723 composites at room temperature, the evolution of fatigue hysteresis loss energy depends upon fatigue peak stress, i.e., under $\sigma_{\max}=280$ MPa, the fatigue hysteresis loss energy of SiC/CAS composite increases first, then decreases with increase of the applied cycles, corresponding to the right and left parts of the hysteresis loss energy versus interface shear stress curve; under $\sigma_{\max}=180$ MPa, the fatigue hysteresis loss energy of SiC/CAS-II composite increases from 5 KPa at the 3rd cycle to 25 KPa at the 3200th cycle, corresponding to the right part of the hysteresis loss energy versus interface shear stress curve; under $\sigma_{\max}=500$ MPa, the fatigue hysteresis loss energy of SiC/1723 composite increases from 25 KPa at the 10th cycle to 38 KPa at the 10011th cycle, corresponding to the right part of the hysteresis loss energy versus interface shear stress curve. For cross-ply SiC/CAS composite, under $\sigma_{\max}=180$ MPa at room temperature, the fatigue hysteresis loss energy increases from 40 KPa at the 10th cycle to 58 KPa at the 1000th cycle, corresponding to the right part of the hysteresis loss energy versus interface shear stress curve.

For cross-ply SiC/MAS-L composite at elevated temperature in inert atmosphere, under $\sigma_{\max}=110$ MPa, the fatigue hysteresis loss energy decreases from 8.3 KPa at the 5th cycle to 4.3 KPa at the 34162th cycle at 800 °C; and from 14 KPa at the 6th cycle to 5.8 KPa at the 133925th cycle at 1000 °C. As the radial thermal residual tensile stress existed in the fiber/matrix interface, the interface shear stress increases with increase of test temperature, the fatigue hysteresis loss energy decreases with increase of the number of applied cycles, corresponding to the left part of the hysteresis loss energy versus interface shear stress curve.

For 2D SiC/SiC composite at elevated temperatures in inert atmosphere, under $\sigma_{\max}=130$ MPa, the fatigue hysteresis loss energy increases from 5.2 KPa at the 15th cycle to 9.4 KPa at the 333507th cycle at 600 °C; from 9 KPa at the 23th cycle to 15.3 KPa at the 97894th cycle at 800 °C; and from 10 KPa at the 22th cycle to 21.8 KPa at the 117055th cycle

at 1000 °C. As the radial thermal residual compressive stress existed in the fiber/matrix interface, interface shear stress decreases with increase of the test temperature, and the fatigue hysteresis loss energy increases with increase of the number of applied cycles, corresponding to the right part of the hysteresis loss energy versus interface shear stress curve.

4 Conclusions

Under cyclic fatigue, the interface shear stress decreases with increase of the number of applied cycles due to interface wear at room temperature or interface oxidation at elevated temperature, leading to the evolution of fatigue hysteresis loss energy versus applied cycles. The theoretical relationship between the hysteresis loss energy, stress–strain hysteresis loops, interfacial frictional slip and interfacial shear stress of fiber-reinforced CMCs have been established. With decrease of the interface shear stress, the hysteresis loss energy increases to the peak first, then decreases to zero KPa. The effects of fatigue peak stress, stress amplitude, fiber volume fraction, matrix crack spacing and matrix cracking mode on the evolution of hysteresis loss energy versus interface shear stress curve have been analyzed.

The evolution characteristics of fatigue hysteresis loss energy versus applied cycles in different types of fiber-reinforced CMCs, i.e., unidirectional C/SiC, SiC/CAS, SiC/CAS–II and SiC/1723, cross-ply C/SiC, SiC/CAS, and SiC/MAS–L, 2D SiC/SiC, 2.5D C/SiC CMCs at room and elevated temperatures, have been investigated. The evolution of fatigue hysteresis loss energy depends upon interface debonding and interface frictional slip between fibers and matrix, fatigue peak stresses, fiber preforms, radial thermal residual stress in fiber/matrix interface, initial interface shear stress, matrix crack spacing and test conditions.

Nowdays, the mainly problem concerning fiber-reinforced CMCs is linked to evaluate the long lifetimes under various loading conditions, test temperatures and atmospheres. The damage mechanisms involved, i.e., interface wear or oxidation of the interphase, matrix multicracking and fibers failure, can be effectively reflected in the energy dissipation of the composite. By analyzing the evolution characteristic of fatigue hysteresis loss energy versus applied cycles, the damage inside of the composite can be monitored or evaluated. The lifetime of the composite can be predicted through establishing the relationship between the energy dissipation and failure criterion.

Acknowledgments The author thanks the Science and Technology Department of Jiangsu Province for the funding that made this research study possible

Compliance with Ethical Standards

Funding This study has received the support from the Science and Technology Department of Jiangsu Province through the Natural Science Foundation of Jiangsu Province (Grant No. BK20140813).

Conflict of Interest The author declares that he has no conflict of interest.

References

1. Naslain, R.: Design, preparation and properties of non-oxide CMCs for application in engines and nuclear reactors: an overview. *Compos. Sci. Technol.* **64**, 155–170 (2004). doi:10.1016/S0266-3538(03)00230-6

2. Schmidt, S., Beyer, S., Knabe, H., Immich, H., Meistring, R., Gessler, A.: Advanced ceramic matrix composite materials for current and future propulsion system applications. *Acta Astronaut.* **55**, 409–420 (2004). doi:10.1016/j.actaastro.2004.05.052
3. DiCarlo, J.A., Van Roode, M.: Ceramic composite development for gas turbine hot section components. *Proc. ASME Turbo Expo Power Land Sea Air* **2**, 221–231 (2006)
4. Stephen, T.: General Electric primes CMC for turbine blades. *Flight International*. <http://www.flightglobal.com/news/articles/general-electric-primes-cmc-for-turbine-blades-349834/> (2010)
5. Zhang, L.T., Cheng, L.F., Luan, X.G., Mei, H., Xu, Y.D.: Environmental performance testing system for thermostructure materials applied in aeroengines. *Key Eng. Mater.* **313**, 183–190 (2006). doi:10.4028/www.scientific.net/KEM.313.183
6. Evans, A.G., Zok, F.W., McMeeking, R.M.: Fatigue of ceramic matrix composites. *Acta Metall. Mater.* **43**, 859–875 (1995). doi:10.1016/0956-7151(94)00304-Z
7. Rouby, D., Reynaud, P.: Fatigue behavior related to interface modification during load cycling in ceramic-matrix fiber composites. *Compos. Sci. Technol.* **48**, 109–118 (1993). doi:10.1016/0266-3538(93)90126-2
8. Fantozzi, G., Reynaud, P., Rouby, D.: Thermomechanical behavior of long fibers ceramic-ceramic composites. *Silic. Ind.* **66**, 109–119 (2001)
9. Marshall, D.B., Evans, A.G.: Failure mechanisms in ceramic-fiber/ceramic-matrix composites. *J. Am. Ceram. Soc.* **68**, 225–231 (1985). doi:10.1111/j.1151-2916.1985.tb15313.x
10. Holmes, J.W., Cho, C.D.: Experimental observation of frictional heating in fiber-reinforced ceramics. *J. Am. Ceram. Soc.* **75**, 929–938 (1992). doi:10.1111/j.1151-2916.1992.tb04162.x
11. Li, L.B.: Fatigue hysteresis behavior of cross-ply C/SiC ceramic matrix composites at room and elevated temperatures. *Mater. Sci. Eng. A* **586**, 160–170 (2013). doi:10.1016/j.msea.2013.08.017
12. Reynaud, P.: Cyclic fatigue of ceramic-matrix composites at ambient and elevated temperatures. *Compos. Sci. Technol.* **56**, 809–814 (1996). doi:10.1016/0266-3538(96)00025-5
13. Fantozzi, G., Reynaud, P.: Mechanical hysteresis in ceramic matrix composites. *Mater. Sci. Eng. A* **521–522**, 18–23 (2009). doi:10.1016/j.msea.2008.09.128
14. Kotil, T., Holmes, J.W., Comninou, M.: Origin of hysteresis observed during fatigue of ceramic-matrix composites. *J. Am. Ceram. Soc.* **73**, 1879–1883 (1990). doi:10.1111/j.1151-2916.1990.tb05239.x
15. Cho, C.D., Holmes, J.W., Barber, J.R.: Estimate of interfacial shear in ceramic composites from frictional heating measurements. *J. Am. Ceram. Soc.* **74**, 2802–2808 (1991). doi:10.1111/j.1151-2916.1991.tb06846.x
16. Pryce, A.W., Smith, P.A.: Matrix cracking in unidirectional ceramic matrix composites under quasi-static and cyclic loading. *Acta Metall. Mater.* **41**, 1269–1281 (1993). doi:10.1016/0956-7151(93)90178-U
17. Ahn, B.K., Curtin, W.A.: Strain and hysteresis by stochastic matrix cracking in ceramic matrix composites. *J. Mech. Phys. Solids* **45**, 177–209 (1997). doi:10.1016/S0022-5096(96)00081-6
18. Solti, J.P., Mall, S., Robertson, D.D.: Modeling damage in unidirectional ceramic-matrix composites. *Compos. Sci. Technol.* **54**, 55–66 (1995). doi:10.1016/0266-3538(95)00041-0
19. Solti, J.P., Mall, S., Robertson, D.D.: Modeling of fatigue in cross-ply ceramic matrix composites. *J. Compos. Mater.* **31**, 1921–1943 (1997). doi:10.1177/002199839703101903
20. Vagaggini, E., Domergue, J.M., Evans, A.G.: Relationships between hysteresis measurements and the constituent properties of ceramic matrix composites: I, Theory. *J. Am. Ceram. Soc.* **78**, 2709–2720 (1995). doi:10.1111/j.1151-2916.1995.tb08046.x
21. Hutchison, J.W., Jensen, H.M.: Models of fiber debonding and pullout in brittle composites with friction. *Mech. Mater.* **9**, 139–163 (1990). doi:10.1016/0167-6636(90)90037-G
22. Li, L.B., Song, Y.D., Sun, Z.G.: Influence of interface de-bonding on the fatigue hysteresis loops of ceramic matrix composites. *Chin. J. Solids Mech.* **30**, 8–14 (2009) (in Chinese)
23. Li, L.B., Song, Y.D., Sun, Z.G., Sun, J.: Effect of fiber Poisson contraction on fatigue hysteresis loops of ceramic matrix composites. *J. Nanjing Univ. Aeronaut. Astronaut.* **41**, 181–186 (2009) (in Chinese)
24. Li, L.B., Song, Y.D.: Effect of fiber failure on quasi-static unloading/reloading hysteresis loops of ceramic matrix composites. *Trans. Nanjing Univ. Aeronaut. Astronaut.* **28**, 94–102 (2011)
25. Li, L.B., Song, Y.D., Sun, Y.C.: Effect of matrix cracking on hysteresis behavior of cross-ply ceramic matrix composites. *J. Compos. Mater.* **48**, 1505–1530 (2014). doi:10.1177/0021998313488149
26. Li, L.B.: Modeling hysteresis behavior of cross-ply C/SiC ceramic matrix composites. *Compos. Part B Eng.* **53**, 36–45 (2013). doi:10.1016/j.compositesb.2013.04.029
27. Kuo, W.S., Chou, T.W.: Multiple cracking of unidirectional and cross-ply ceramic matrix composites. *J. Am. Ceram. Soc.* **78**, 745–755 (1995). doi:10.1111/j.1151-2916.1995.tb08242.x
28. Zawada, L.P., Butkus, L.M., Hartman, G.A.: Tensile and fatigue behavior of silicon carbide fiber-reinforced aluminosilicate glass. *J. Am. Ceram. Soc.* **74**, 2851–2858 (1991). doi:10.1111/j.1151-2916.1991.tb06854.x

29. Opalski, F.A., Mall, S.: Tension-compression fatigue behavior of a silicon carbide calcium-aluminosilicate ceramic matrix composite. *J. Reinf. Plast. Compos.* **13**, 420–438 (1994). doi:[10.1177/073168449401300503](https://doi.org/10.1177/073168449401300503)
30. Yang, F.S.: Research on fatigue behavior of 2.5d woven ceramic matrix composites. Master Thesis, Nanjing: Nanjing University of Aeronautics and Astronautics (2011) (in Chinese)
31. Dalmaz, A., Reynaud, P., Rouby, D., Fantozzi, G., Abbe, F.: Mechanical behavior and damage development during cyclic fatigue at high-temperature of a 2.5D carbon/sic composite. *Compos. Sci. Technol.* **58**, 693–699 (1998). doi:[10.1016/S0266-3538\(97\)00150-4](https://doi.org/10.1016/S0266-3538(97)00150-4)